Structural Eng. / Earthquake Eng. Vol. 7. No. 1, 55s-65s. April 1990
Japan Society of Civil Engineers (Proc. of JSCE No. 416/I-13)

AN ELASTO-PLASTIC LARGE DEFORMATION ANALYSIS OF COMPRESSED CYLINDRICAL SHELLS WITH INITIAL IMPERFECTIONS

By Shobha R. GUNAWARDENA and Tsutomu USAMI***

The behavior of axially loaded cylindrical shells is studied using a general purpose non-linear shell element. The well-known nine-node degenerated shell element was selected among the variety of shell finite elements proposed and developed in the past by several researchers, because it satisfies all the compatibility conditions between adjacent elements directly and gives accurate results. The behavior of axially loaded cylindrical shells are observed through computations of some fabricated pipes which were tested in Nagoya University. The measured initial imperfections are included in the calculations. The effects of initial imperfections on the cylinder strength are also discussed.

Keywords : elasto-plastic, large deformation, degenerated shell element, cylindrical shells, initial imperfections

1. INTRODUCTION

During the past two decades, the behavior of axially loaded compressed cylindrical shells has been examined, experimentally and theoretically, to verify the initial imperfection sensitivity on the strength. The research work done by J. E. Harding[1)~3)] has made a considerable effort to explain the effects of initial deflections, residual stresses, cylinder length, radius-thickness ratio, etc. But the subject is still to be investigated as, due to the authors' knowledge, there is a little work done to compare the theoretically computed results, using the measured initial imperfections, with experiments done on axially loaded cylindrical shells because of the difficulty of measuring the initial imperfections incurred in the test. The initial deflections and the residual stresses are different for each problem and, without a clear knowledge of those, difficult to correlate.

To detect the ultimate strength and the buckling mode, for the further examination of the behavior, an elasto-plastic large deformation analysis must be done. In a review on available finite elements it is understood that the nine-node degenerated shell element with reduced integration is more effective and accurate over the other shell elements. The formulations presented by K. J. Bathe *et al.*[4)~6)] are used and all the necessary transformations to include the large deformation effects are done additionally. Among the number of problems solved, some typical examples will be presented first to show the ability of the element developed in handling geometrically and materially non-linear problems. Some laboratory tests done in Nagoya University on axially loaded cylindrical shells are computed and discussed in detail to see the effects on initial imperfections.

* M. Eng., Graduate student, University of California (Santa Barbara, California, U. S. A.)
** Member of JSCE, Dr. Sc., Dr. Eng., Professor of Civil Engineering, Nagoya University (Chikusa-Ku, Nagoya 464)

2. FORMULATION OF EQUILIBRIUM EQUATION

The notations used are similar to Ref. 5), as follows if explained briefly,

Left subscript; Configuration with respect to which the quantity is measured.

Left superscript; Configuration in which the quantity occurs.

No superscript; increment of the quantity.

The principle of virtual displacement with updated Lagrangian formulation is employed. The basic equation to be solved is,

$$\int_{tV} ({}^{t+\sigma t}_{t}S_{ij})\,\delta\,({}^{t+\sigma t}_{t}\varepsilon_{ij})\,{}^{t}dV = {}^{t+\sigma t}\Re \quad \cdots\cdots (1)$$

where ${}^{t+\sigma t}_{t}S_{ij}$=2nd Piola-Kirchhoff stress tensor, ${}^{t+\sigma t}_{t}\varepsilon_{ij}$=Green strain tensor, ${}^{t+\sigma t}\Re$=External virtual work, ${}^{t}V$=Volume of the body at configuration t.

The above quantities are referred to the previous state as follows,

$${}^{t+\sigma t}_{t}S_{ij} = {}^{t}\tau_{ij} + {}_{t}S_{ij}, \quad {}^{t+\sigma t}_{t}\varepsilon_{ij} = {}_{t}e_{ij} + {}_{t}\eta_{ij}, \quad {}_{t}S_{ij} = {}_{t}C_{ijrs}\,{}_{t}\varepsilon_{rs} \quad \cdots\cdots (2\cdot a\sim c)$$

in which ${}^{t}\tau_{ij}$ is the Cauchy stress tensor, ${}_{t}S_{ij}$ is the increment in stress at configuration t, ${}_{t}C_{ijrs}$ is the corresponding constitutive relation at configuration t, ${}_{t}e_{ij}$ and ${}_{t}\eta_{ij}$ are the linear and nonlinear strain increment tensors, respectively.

Substitution of Eq. (2) in Eq. (1) and linearization of the left hand side by ${}_{t}S_{ij} = {}_{t}C_{ijrs}\,{}_{t}e_{rs}$ leads to the final equation given below (written in matrix form).

$$[[{}^{t}_{t}K_{L}] + [{}^{t}_{t}K_{NL}]]\,\{{}_{t}U\} = \{{}^{t+\sigma t}R\} - \{{}^{t+\sigma t}_{t+\sigma t}F\} \quad \cdots\cdots (3)$$

where $[{}^{t}_{t}K_{L}]$=linear stiffness matrix, $[{}^{t}_{t}K_{NL}]$=nonlinear stiffness matrix, $\{{}_{t}U\}$=displacement increment vector, $\{{}^{t+\sigma t}R\}$=vector of external nodal point forces applied, $\{{}^{t+\sigma t}_{t+\sigma t}F\}$=vector of nodal point forces obtained from internal forces.

3. ISOPARAMETRIC FORMULATION

The geometry of the shell is described by the coordinates and direction cosines of the normal vectors at the nodal points on the shell mid surface. Fig. 1 gives an illustration of the element. The interpolation function used for the geometry is given by

$${}^{t}X_i = \sum_{k=1}^{9} (h_k)({}^{t}X_i^k) + \frac{t}{2}\sum_{k=1}^{9} (h_k)(a)({}^{t}V_{ni}^k) \quad \cdots\cdots (4)$$

where ${}^{t}X_i^k$=global coordinate of node k, ${}^{t}X_i$=global coordinate at a generic point on the shell, h_k=shape function on r-s plane associated with node k, a=thickness of the shell, ${}^{t}V_{ni}^k$=component i of the unit normal vector, ${}^{t}\vec{V}_n^k$, to the mid-surface of the element at node k.

The displacement increment ${}_{t}u_i$ is given by ${}_{t}u_i = {}^{t+\sigma t}X_i - {}^{t}X_i$, which leads to

$${}_{t}u_i = \sum_{k=1}^{9} (h_k)({}_{t}u_i^k) + \frac{t}{2}\sum_{k=1}^{9} (h_k)(a)({}_{t}V_{ni}^k) \quad \cdots\cdots (5)$$

where, ${}_{t}V_{ni}^k = {}^{t+\sigma t}V_{ni}^k - {}^{t}V_{ni}^k$. Initial values of ${}^{t}\vec{V}_n^k$, ${}^{0}\vec{V}_n^k$, are computed as follows:

$${}^{0}\vec{V}_n^k = \left(\frac{\partial\,{}^{0}\vec{X}^k}{\partial r} \times \frac{\partial\,{}^{0}\vec{X}^k}{\partial s}\right) \Big/ \left|\frac{\partial\,{}^{0}\vec{X}^k}{\partial r} \times \frac{\partial\,{}^{0}\vec{X}^k}{\partial s}\right| \quad \cdots\cdots (6)$$

Two orthonormal vectors to ${}^{t}\vec{V}_n^k$ are selected as follows (see Fig. 1):

$${}^{t}\vec{V}_1^k = (\vec{X}_2 \times {}^{t}\vec{V}_n^k)/|\vec{X}_2 \times {}^{t}\vec{V}_n^k| \;;\; {}^{t}\vec{V}_2^k = {}^{t}\vec{V}_n^k \times {}^{t}\vec{V}_1^k \quad \cdots\cdots (7)$$

In Eq. (7), $\vec{X}_2$ represents a unit vector in global X_2 direction. In the special case that ${}^{t}\vec{V}_n^k$ is parallel to $\vec{X}_2$, ${}^{t}\vec{V}_1^k$ and ${}^{t}\vec{V}_2^k$ are taken as $\vec{X}_3$ and $\vec{X}_1$. If any initial boundary conditions or loading conditions are given in these two local

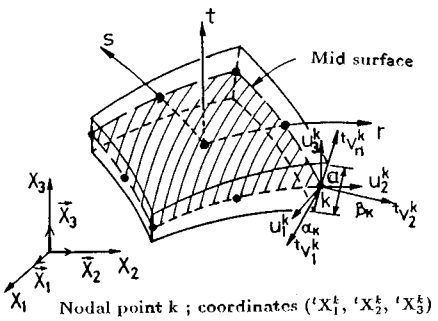

Fig. 1 Nine-node shell element.

degrees of freedoms one must be careful in selecting the global coordinate system ; the vector $\vec{X}_2$ must not become perpendicular to the shell surface at such loaded or restrained points throughout the application of load (displacement) increments.

The components of the ${}^{t+\delta t}\vec{V}_n^k$ can be written in terms of ${}^tV_{1i}^k$, ${}^tV_{2i}^k$ and the rotations α_k, β_k of ${}^t\vec{V}_n^k$ about ${}^t\vec{V}_1^k$ and ${}^t\vec{V}_2^k$ respectively[9],

$$ {}^{t+\delta t}V_{ni}^k=0.5(\sin\beta_k\cos\alpha_k+\sin\beta_k){}^tV_{1i}^k-0.5(\sin\alpha_k\cos\beta_k+\sin\alpha_k){}^tV_{2i}^k +\cos\beta_k\cos\alpha_k{}^tV_{ni}^k \quad (8) $$

For small α_k and β_k, $\cos\alpha_k\approx\cos\beta_k\approx1.0$, $\sin\alpha_k\approx\alpha_k$, and $\sin\beta_k\approx\beta_k$. Then

$$ {}^{t+\delta t}V_{ni}^k=\beta_k{}^tV_{1i}^k-\alpha_k{}^tV_{2i}^k+{}^tV_{ni}^k \quad (9) $$

Eq. (9) is used in the finite element formulation assuming α_k and β_k are small enough. But in the calculation of ${}^{t+\delta t}V_{ni}^k$, Eq. (8) is used to ensure the unity of the vector $\vec{V}_n^k$ throughout the loading. Eq. (5) can then be rewritten as follows :

$$ {}_tu_i=\sum_{k=1}^{9}(h_k)({}_tu_i^k)+\frac{t}{2}\sum_{k=1}^{9}(h_k)(a)(-{}^tV_{2i}^k\alpha_k+{}^tV_{1i}^k\beta_k) \quad (10) $$

The local derivatives of the displacement increments are computed directly from the Eq. (10) and then transformed to the global derivatives using the Jacobian transformation. The linear and non-linear incremental strain-displacement relations, which are used in the computations of stiffness matrix and unbalanced force vector, can be directly written in terms of obtained global derivatives of displacement increments.

4. CONSTITUTIVE RELATION

In this study an isotropic, elasto-plastic material behaviour is modeled. Von Mises yield criteria and isotropic hardening are used with the associated flow rule. The effects of elastic unloading are incorporated in the analysis following the procedures found in Ref. 20).

The shell assumption that the stress normal to the shell is zero, is imposed in the usual three dimensional constitutive law corresponding to a local coordinate system. The resulting matrix is transformed to the global coordinate system as the calculations of all the other quantities are performed with respect to that system. The $\vec{V}_n$, $\vec{V}_1$, $\vec{V}_2$ system, which is, however, calculated for previous formulations, is taken as the local coordinate system.

In the elasto-plastic stress-strain relation the local Cauchy stresses are used to impose the large deformation effects. In obtaining the stresses for the current configuration using the previous state, the Eq. (2·a) is used. The stresses ${}^{t+\delta t}_tS_{ij}$ are transformed to ${}^{t+\delta t}\tau_{ij}$ for each point as follows.

$$ {}^{t+\delta t}\tau_{mn}=\frac{{}^{t+\delta t}\rho}{{}^t\rho}\left(\frac{\partial\,{}^{t+\delta t}X_m}{\partial\,{}^tX_i}\right){}^{t+\delta t}_tS_{ij}\left(\frac{\partial\,{}^{t+\delta t}X_n}{\partial\,{}^tX_j}\right) \quad (11) $$

where ${}^{t+\delta t}\rho/{}^t\rho$ is the ratio of mass densities at configurations t and $t+\delta t$ and is given by the determinent of $(\partial\,{}^{t+\delta t}X_i/\partial\,{}^tX_j)$.

5. NUMERICAL INTEGRATION

It is observed that the reduced integration on the surface of the shell gives effective and accurate solutions over the full integration. The 2×2 Gauss-Legendre integration is done on the surface. In the case of elasto-plastic analysis a fine mesh is necessary to capture the plastic zone. Since the large deformations are to be considered, the stresses along the thickness direction do not remain constant. Therefore the thickness is devided to some layers, where the stresses can be assumed constant, and integrated using Simpson's rule. The number of layers can be defined as a data (2~8).

6. SOLUTION METHOD

Displacement increment using the modified Newton-Raphson method is adopted in the computations of this study. But the developed element routine has the capability of handling the solutions using the modified arc length method also. The popular research tool FEAP[7),8)] was used to perform the basic finite element procedures. In that package there is a facility to perform iterative solutions with a check of displacement convergence. Whenever $\|_t u_i\| \leqq \mathrm{TOL}$. $\max_j \|^t u_j\|$, $j=1, 2, \cdots\cdots, i$, the iteration ceases and the next load/displacement step will be started. Here $\|_t u_i\|$ is the norm of the displacement vector at i-th iteration and TOL. is a predefined tolerance for displacements.

The computer machine FACOM M-780 was used for all the computations in this study.

7. NUMERICAL EXAMPLES

(1) Example 1 Rectangular beam with clamped edges subjected to a concentrated load at mid span

The problem is illustrated in Fig. 2. Perfectly plastic material behaviour is used with yield stress, σ_y, of 1 000 kgf/cm^2, Poisson's ratio, ν, of 0.17 and Young's modulus, E, of 200 000 kgf/cm^2. Five equal elements were used in half span and the load-displacement curve obtained (Fig. 2) is in very good agreement with the result of Ref. 10) which was computed from 50 beam elements in half span. There was a difficulty of convergence near the peak load. 50 displacement increments of 0.2 cm with 10^{-3} tolerance was necessary to solve the problem.

(2) Example 2 Plate in uniform edge displacement

The problem is described in Fig. 3. Finite element mesh of 2×2 elements was used to analyze a quater of the plate for symmetry. An initial deflection w of

$$w = w_0 \sin\left(\frac{\pi x}{a}\right) \sin\left(\frac{\pi y}{b}\right) \cdots\cdots (12)$$

was applied in the out-of-plane direction, where w_0 is the maximum value of w. In elastic-only-analysis, 60 displacement increments of 0.002 mm was given with a tolerance of 10^{-3}. The result was compared with the result in Ref. 11) and shown in Fig. 3. In the figure, σ_y=yield stress, E=Young's modulus, ν=Poisson's ratio, a=plate length, b=plate width, t=plate thichness, and p=reaction force at the loaded edges. The computation time was about 40 seconds. In elasto-plastic analysis similar displacement increments were given with a tolerance of 10^{-4}. The computation time was about 98 seconds. The result agrees with the results of Ref. 12). The plate behaviour changed from elastic to elasto-plastic at 22nd displacement step ($\varepsilon/\varepsilon_y$=0.64).

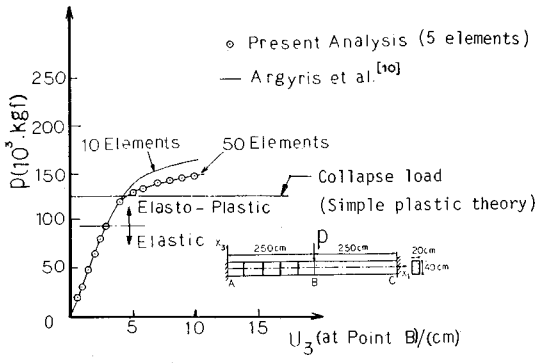

Fig. 2 Schematic representation and load-mid span displacement curve for beam with clamped edges.

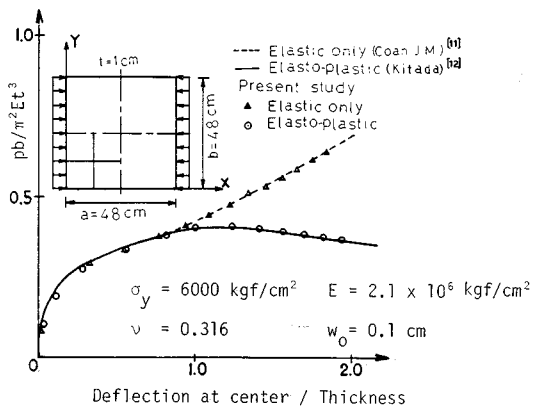

Fig. 3 Plate with inplane loading.

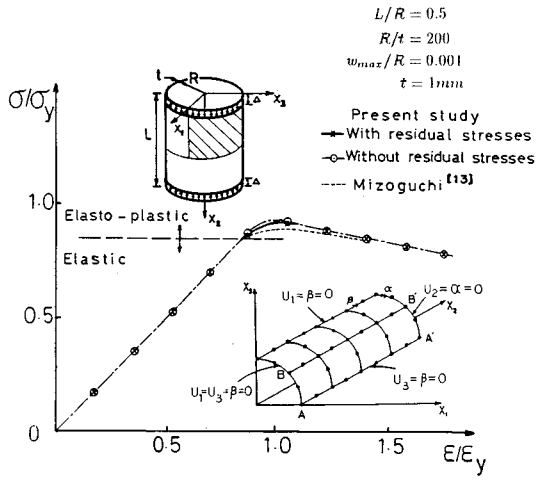

Fig. 4 Average stress-average strain curve for axially loaded cylindrical shell.

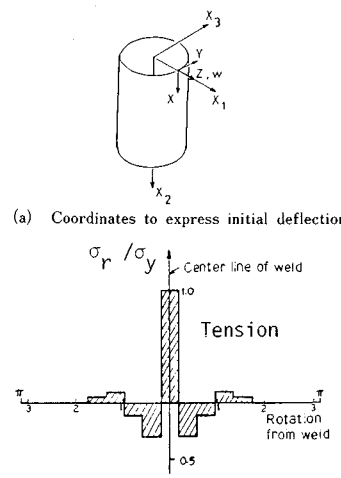

(a) Coordinates to express initial deflection

(b) Assumed residual stress

Fig. 5 Initial imperfections.

(3) Example 3 Axially loaded cylindrical shell with initial imperfections

The illustrated problem in Fig. 4 was solved prior to the computations of the cylindrical shells tested in the laboratory to ensure the ability of the developed element in handling axially loaded cylindrical shells. The initial deflection, w, used is,

$$w = w_{\max} \sin\left(\frac{\pi x}{L}\right) \cos\left(\frac{4y}{R} - \frac{\pi}{2}\right) \quad \cdots\cdots (13)$$

where $w_{\max}$=maximum value of w, L=shell length, R=radius of shell, and x, y=coordinates defined in Fig. 5(a).

50 displacement increments of 0.002 mm were applied with a tolerance of 10^{-3}. The average stress (σ)-average strain (ε) curve (Fig. 4) was compared with the solution of Ref. 13). The dynamic relaxation method has been used in Ref. 13) with the thin shell theory of Sanders[21]. Assuming symmetry about the horizontal mid surface, a half and a quater of the upper half of the cylinder was analyzed simultaneously. The results obtained were very closer to each other. The reason of this similarity may be the symmetry of the initial imperfection along the circumference (out of roundness). The computation time was about half for the latter case (255 sec. and 120 sec.). The analysis was done with and without residual stresses, the distribution of which is as shown in Fig. 5(b). The effect observed was only 0.7 % on the ultimate strength.

The shell buckles near the top end surface. Fig. 6(a) illustrates the chnage in outward displacement along the axial direction with respect to the initial position. Due to the evenness of the initial conditions the variation is similar at different sections. It can be seen that the outward displacement is extremely localized near the end of the shell.

A sketch of the plastic zone developed at $\varepsilon/\varepsilon_y = 1.74$ is presented in Fig. 6(b). This diagram was drawn by observing the material property changes at each integration point as the displacement was increased gradually (up to $\varepsilon/\varepsilon_y = 1.74$). Some parts of the cylinder started yielding from the inner surface and some parts yielded from outer surface while the other portions remained as elastic. A clear relation can be seen between Figs. 6(a) and (b). Yielding starts from the inner surface of the cylinder (at $\varepsilon/\varepsilon_y = 0.85$), under compression, in the vicinity of the region with maximum outward displacement and penetrates into the outer surface at $\varepsilon/\varepsilon_y = 1.74$. The cylinder yields from the outer surface at a height where the outer surface is in compression.

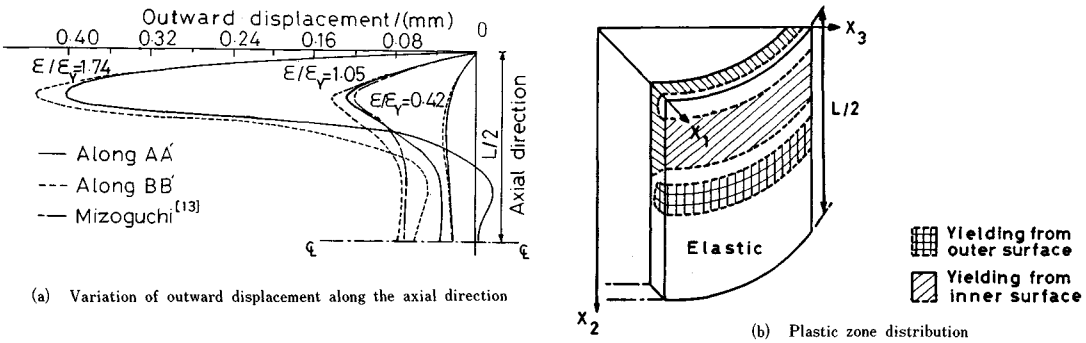

(a) Variation of outward displacement along the axial direction

(b) Plastic zone distribution

Fig. 6 Axially loaded cylindrical shell.

(4) Example 4 Comparison with test results - axially loaded cylindrical shells

Four cylindrical shells tested in Nagoya University[14] were analyzed. The geometrical and material properties of the specimens are as in Table 1.

a) Initial imperfection

The imperfections of the specimens are uneven and difficult to measure because of the curvature of the cylindrical shell. There is no clear reference of perfect shape for curved elements as for straight of flat elements after those are deformed. The method used in Ref. 15) was used to tackle this problem. In that study a Fourier analysis was done to calculate the initial deviations from the perfect cylinder at any point using the measured values at some known points. The initial shape of the developments of four cylinders are shown in Fig. 7. The effect of the residual stress is neglected in this analysis.

b) Boundary conditions

Restrained conditions equivalent to diaphragm walls at top and bottom ends of the cylinder were imposed ($u_1=u_2=\beta=0$ at the top and bottom). The displacement increments were applied as in Example 3. All the problems were solved up to 60 displacement steps.

c) Analytical results and comparison

The specimen NO : 1 did not converge when analyzed with all the imperfections. So only the measurements of the out of roundness was employed with an assumed half sine wave along the axial direction. For the symmetry half of the cylinder was analyzed. A description of finite element meshes and displacement increments with a comparison of computed and test results is given in Table 2.

As it is illustrated in Fig. 8, the computed peak stresses are little higher than the experimental ones. The test curves seem to be deviating from the linear behaviour as early as $\varepsilon/\varepsilon_y=0.3$. In the analysis of specimen NO : 2, yielding starts around the 16th displacement increment ($\varepsilon/\varepsilon_y=0.56$).

d) Buckled shape

Fig. 9 shows 3-dimensional views of the deformed cylinders which were observed in the laboratory. The variations of outward displacement, without initial deflections, along the circumference and axial direction are drawn seperately in Fig. 10 to illustrate the computed results. The variation holds a symmetric pattern with four outward lobes along the circumference except for the specimen NO : 1. In the case of specimen NO : 1 ($R/t=37.5$), no lobes were observed along the circumference. One vertical section for each specimen is presented to exhibit the variation in axial direction.

The buckling modes of specimens NO : 1 and NO : 4 resemble the test results. In specimen NO : 2, computed outward displacements are localized to the bottom diaphragm, in contrary to the experimental result. Another important fact observed is the difference between the deformed shapes of two specimens NO : 2 and NO : 3 which are almost the same in dimensions (i.e., $R/t\approx 56$). This must be clearly an effect of different initial imperfections employed.

CPU time for each problem is given in Table 2. From the solution of specimen NO : 1 it can be said that

Table 1 Geometrical and material properties.

Specimen No:	L (mm)	R (mm)	t (mm)	Area (mm^2)	R/t
NO:1	373	179.79	4.8	5350	37.5
NO:2	552	269.64	4.84	8130	55.7
NO:3	553	270.03	4.77	8020	56.6
NO:4	642	315.28	4.84	9510	65.1
$E=2.119\times 10^4$ kgf/mm^2			$\nu=0.223$		
$\sigma_y=54.84$ kgf/mm^2					

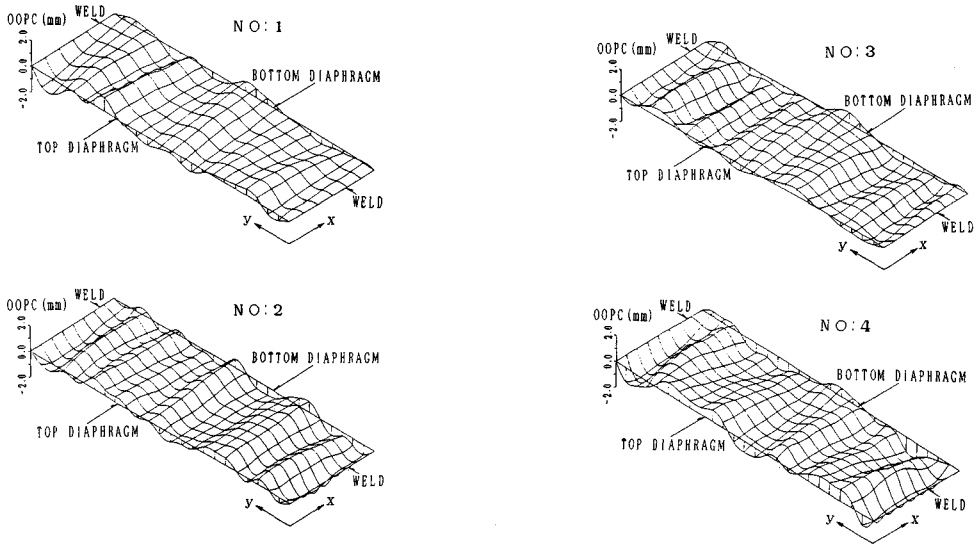

Note : OOPC—Outward displacement Of Perfect Cylinder

Fig. 7 Initial deflection patterns for test specimens[15].

Table 2 A description of finite element models and results.

Specimen NO:	No. of elements	Displacement increment(mm)	σ_u (kg/mm^2) Computed	σ_u (kg/mm^2) Test result	CPU time (sec)
NO:1	32 (4×8)	0.020	53.42	48.5	1567
NO:2	48 (6×8)	0.025	54.09	49.8	1800
NO:3	48 (6×8)	0.025	54.29	47.6	1680
NO:4	48 (6×8)	0.03	53.85	47.8	1611

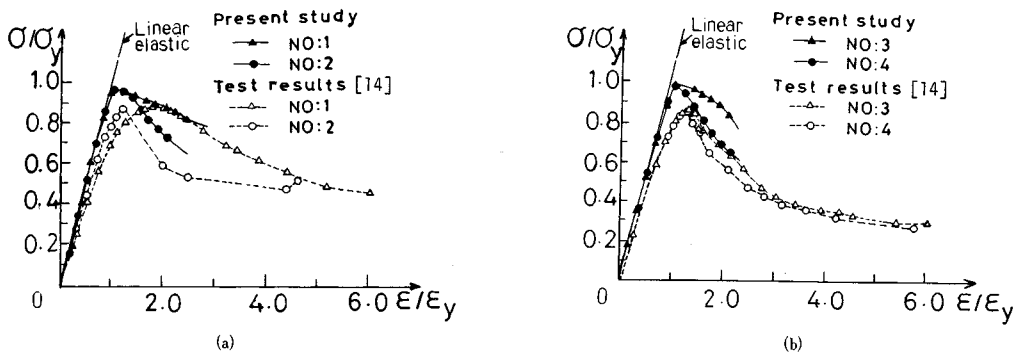

Fig. 8 Comparison of average stress-average strain curves with experimental results[14].

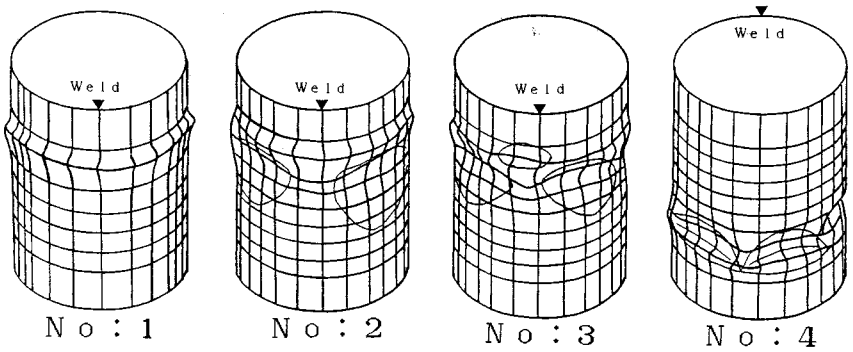

Fig. 9 Three dimensional views of the deformed cylinders (Test results[14]).

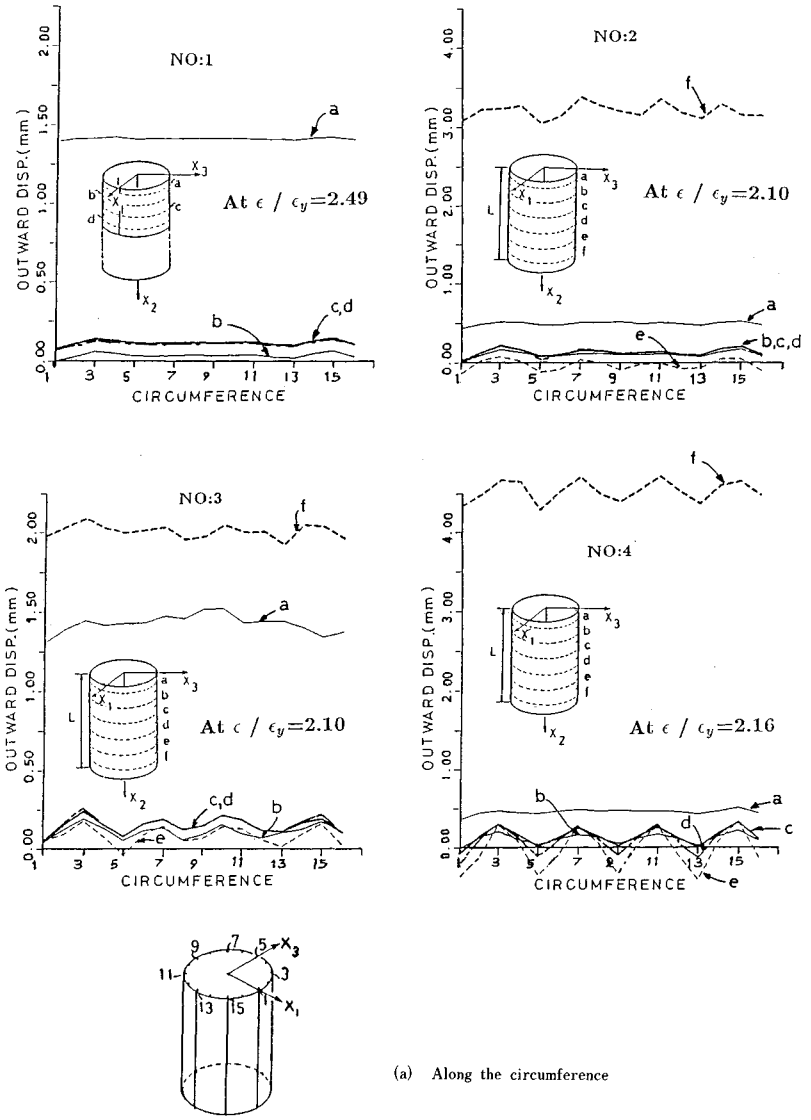

(a) Along the circumference

Fig. 10 The variations of outward displacement.

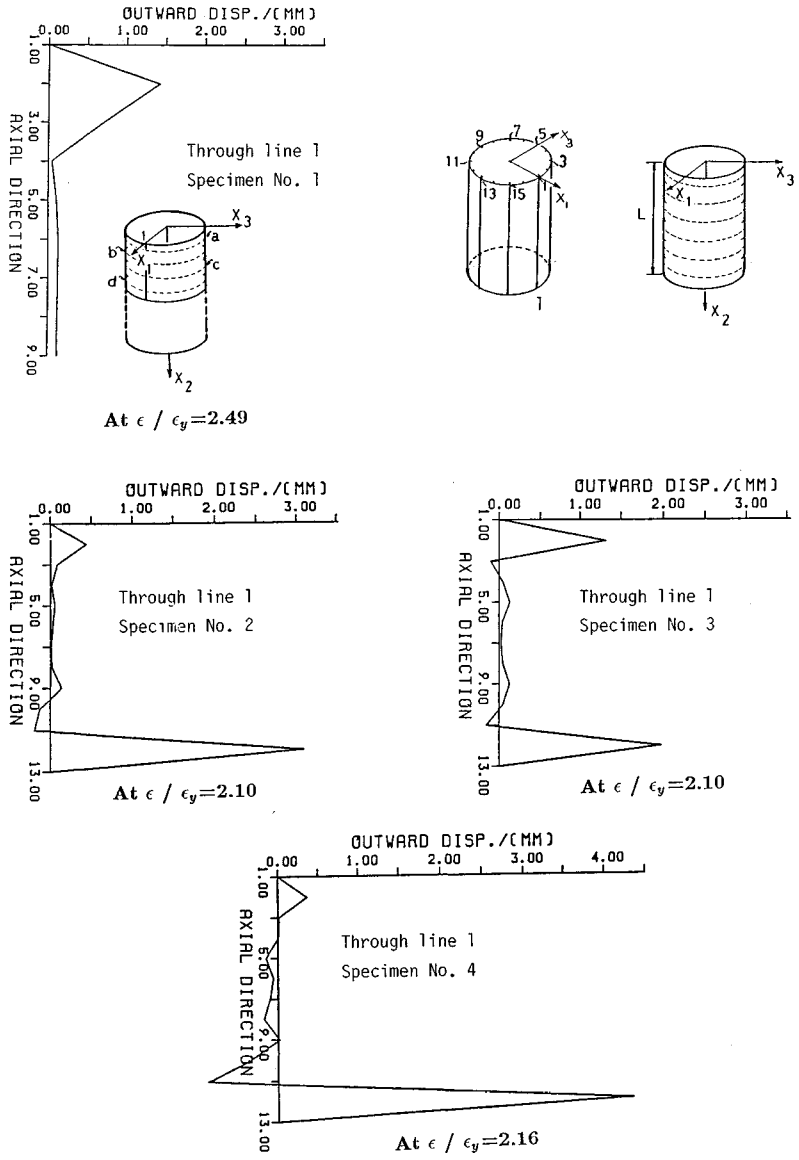

(b) Along the axial direction

Fig. 10 The variations of outward displacement (continued).

all the imperfections need not be imposed to get a reasonable solution. But without knowing what factors basically affect the strength of the cylinder it is harmful to do such assumptions. In the other three specimens buckling occurred near the top or bottom diaphragm (not symmetric about the mid section as it was assumed in the specimen NO : 1).

(5) Example 5 Effect of R/t ratio and the magnitude of initial deflection on the ultimate strength

Here five cylindrical shells with R/t ratio varying from 50 to 200 are each solved twice with two sets of initial deflections as shown in Fig. 11. The boundary conditions are the same as those of Example 3. The initial imperfection mode of $w=w_{\max}\sin(\pi X/L)$ is assumed with the same notations as in Example 3. The magnitude of $w_{\max}$ of Case 2 is obtained by giving the maximum fabrication tolerance specified in

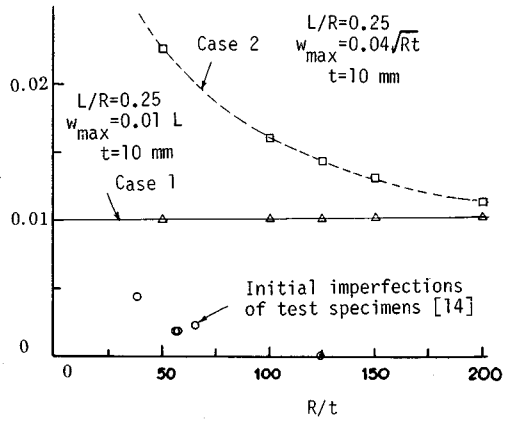

Fig. 11 Comparison of magnitudes of initial deflection.

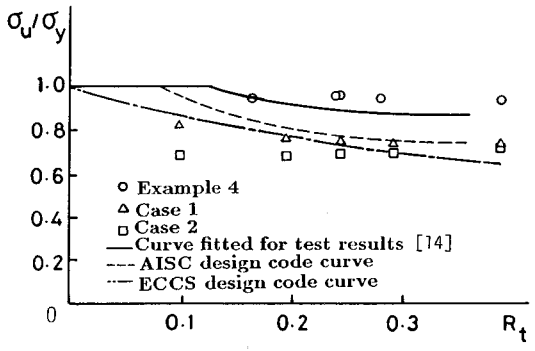

Fig. 12 Comparison of obtained strength curves with design code curves.

ECCS code[17]. It is seen that the initial deflections observed in the Nagoya University test program are much smaller than the fabrication tolerance of ECCS. The parameter R_t[18] was drawn versus σ_u/σ_y to illustrate the result (Fig. 12), where

$$R_t=1.65\frac{\sigma_y}{E}\frac{R}{t} \quad \cdots\cdots (14)$$

The points obtained from Examples 4 and 5 are also plotted in the same diagram. The computed strengths for test specimens are lying above the AISC[16] design code curve and the experimental curve[14] while the curves of Case 1 and Case 2 lie below those. Results of Case 1 are in good agreement with ECCS[17] strength curve. However, the ECCS strength curve is found to be optimistic for initial deflections of Case 2. The solid curve has been obtained from the Nagoya University tests[14] as well as the tests of Lehigh University[19]. Therefore it may be though of that initial deflections observed in actual fabricated pipes are much smaller than those specified in ECCS (or Case 2 initial deflections). It can be concluded from the Figs. 11 and 12 that the ultimate strengths are higher for smaller magnitudes of initial deflections (tested specimens) and lower for larger initial deflections (Case 1 and Case 2).

8. CONCLUSIONS

The post-buckling behavior of axially loaded cylindrical shells was studied using a nine-node degenerated, isoparametric shell element. Both initial deflections of shell surface and residual stresses caused by welding are included in the analysis. From the extensive numerical study, the following conclusions have been drawn :

(1) The developed element has the ability of solving a variety of non-linear shell problems with high accuracy.

(2) The outward displacements of compressed cylindrical shells are localized near their ends regardless of the initial imperfection pattern along the axial direction.

(3) The residual stresses found for fabricated tubes are less effective on the ultimate strength.

(4) The initial deflection mode affects the buckling mode as well as the load-deformation characteristics in the post-critical range.

(5) The maximum strengths are, however, less sensitive to the initial deflection mode.

(6) The ECCS strength curve for cylindrical shell in compression is found to be optimistic for the maximum initial deflection specified in the rule.

REFERENCES

1) Harding, J. E. : The elasto-plastic analysis of imperfect cylinders, Proc. of Institution of Civil Engrs., Part 2, pp. 875-892, Dec., 1978.
2) Harding, J. E. : Ring stiffened cylinders under axial and external pressure loading, Proc. of Institution of Civil Engrs., Part 2, pp. 863-878, Sep., 1981.
3) Estefen, S. F. and Harding, J. E. : Ring stiffener behaviour and its interaction with cylindrical panel buckling, Proc. of Institution of Civil Engrs., Part 2, pp. 243-264, June, 1983.
4) Bathe, K. J. and Bolourchi, S. : A Geometric and Material non-linear plate and shell element, Computers & Structures, Vol. 11, pp. 23-48, 1980.
5) Bathe, K. J. : Finite Element Procedures in Engineering Analysis, Prentice-Hall, Englewood cliffs, New Jersey, 1982.
6) Bathe, K. J., Ramm, E. and Wilson, E. L. : Finite element formulations for large deformation dynamic analysis, Int. Journal for Numerical Methods in Engineering, Vol. 9, pp. 353-386, 1975.
7) Taylor, R. L. : Computer procedures for finite element analysis, Zienkiewicz, O. C., The Finite Element Method, 3rd Edition, pp. 677-773, 1979.
8) Kanok-Nukulchai, W. : FEAP 81-Finite Element Analysis Program, Asian Institute of Technology, Devision of Structural Engineering and Construction, 1981.
9) Surana, K. S. : Geometrically nonlinear formulation for the curved shell elements, Int. Journal for Numerical Methods in Engineering, Vol. 19, pp. 581-615, 1983.
10) Argyris, J. H. *et al.* : Natural analysis of elasto-plastic frames, Computer Method in Applied Mechanics and Engineering, Vol. 35, 1982.
11) Coan, J. M. : Large deflection theory for plates with small initial curvature loaded in edge compression, Journal of Applied Mechanics, Vol. 18, pp. 143-151, 1951.
12) Kitada, T. : Study on ultimate strength of steel plates and stiffened plate under compression, D. Eng. thesis presented to Osaka University, 1980.
13) Mizoguchi, H. : Application of dynamic relaxation method to nonlinear analysis of plate and circular cylindrical shell, Master's thesis, Department of Civil Engineering, Nagoya University, 1983.
14) Usami, T., Aoki, T., Kato, M. and Wada, M. : Test on the compressive and bending strength of steel tubular members, Proc. of JSCE (in press).
15) Wada, M., Aoki, T., Usami, T. and Mizuno, E. : A method of measuring initial imperfections of short fabricated tubes (in preparation).
16) AISC (American Institute of Steel Construction) : Specification for the design, fabrication and erection of structural steel for buildings, 1978.
17) ECCS (European Convention for Constructional Steelwork) : European recommendations for steel construction, Publication No. 29, Buckling of shells, 1983.
18) Nishino, F. ed. : Design code for steel structures——PART A Structures in general——, Publication of the Committee on steel structures, JSCE, Nov., 1987.
19) Alexis, O. and Stephen, X. G. : Local buckling tests on three steel large diameter tubular columns, Department of Civil Engineering, Fritz Engineering Laboratory, Lehigh University, Bethlehem, Pennsylvania, June, 1977.
20) Owen, D. R. J. and Hinton, E. : Finite Elements in Plasticity, Pineridge Press, 1980.
21) Brush, D. O. and Almroth, B. O. : Buckling of Bars, Plates, and Shells, McGraw-Hill, 1975.

(Received May 8 1989)